Parametric Study of a Finite-Time Steady Flow Reversed Lenoir Refrigeration Cycle

Anand Pai, Chandrakantha Bekal, Manjunath Shetty, and Satish Shenoy B.*

***Abstract*—Ideal reversed heat engine cycles have long been the benchmark for refrigeration systems globally. By applying the concept of finite-time thermodynamics to ideal power and refrigeration cycles, researchers have modeled irreversible cycles that closely emulate real-world operations. In this study, a parametric analysis of the finite-time reversed Lenoir cycle was conducted, representing the first exploration of this reversed cycle using this approach. Key output parameters, such as the coefficient of performance (COP) and power input to the refrigeration cycle, were investigated. The analysis covered critical performance factors, including heat exchanger design, fluid properties, ambient conditions, and state values of the reversed Lenoir cycle, all of which impact the power input $\dot{W}$ and the COP of the finite time reversed Lenoir cycle, COP_{LR}. Additionally, an irreversible compression efficiency was incorporated to account for the various internal and external irreversibilities encountered during the cycle. The study examined the balance between a stable COP_{LR} across different values of the higher heat exchanger effectiveness, ϵ_H (hot side) and ϵ_L (cold side), and the marginal enhancement in COP_{LR} at elevated pressure ratios π, ranging from 4 to 7. Furthermore, the cycle operation was compared with the well-established reversed Brayton cycle to evaluate performance parameters.**

***Index Terms*—Reversed Lenoir Cycle, Refrigeration, Irreversibility, Finite Time Thermodynamics, Coefficient of Performance, Reversed Brayton Cycle.**

NOMENCLATURE

A_s	Heat exchanger surface area (m^2)
COP_B	Coefficient of Performance of the reversed Brayton cycle
COP_{LR}	Coefficient of performance of the reversed Lenoir cycle
C_{air}	Heat Capacity of the refrigerant (air) = 2 kg/s × 1.005 kJ/kg/K = 2.01 (kW/K)
C_{max}	Maximum heat capacity of the fluid (kJ/K)
C_{min}	Minimum heat capacity of the fluid (kJ/K)
C_r	Capacity ratio
N_H	Number of transfer units for the hot side heat exchanger
N_L	Number of transfer units for the cold side heat exchanger
T_1	Temperature at compressor inlet (K)
T_2	Temperature at compressor outlet (K)
T_C	Condenser Temperature (K)
T_E	Evaporator Temperature (K)
T_H	Source Temperature (K)
T_L	Sink Temperature (K)
$T_{1'}$	Temperature at the outlet of the isobaric heat gain process 4'-1' (K)
$T_{2'}$	Temperature at the inlet of the isobaric heat loss process 2'-3' (K)
T_{2S}	Temperature at compressor outlet considering Irreversible loss (K)
$T_{3'}$	Temperature at the outlet of the isobaric heat loss process 2'-3' (K)
$T_{4'}$	Temperature at the inlet of the isobaric heat gain process 4'-1' (K)
U	Overall heat transfer coefficient of the heat exchanger (W/m^{2}K)
U_H	Overall heat transfer coefficient of the hot side heat exchanger (W/m^{2}K)
U_L	Overall heat transfer coefficient of the cold side heat exchanger (W/m^{2}K)
ΔT_{lm}	Logarithmic mean temperature difference (K)
$\dot{Q}$	Rate of heat transfer (kW)
$\dot{Q}_1$	Heat rejected during process 2-3 (kW)
$\dot{W}$	Power input to the reversed Lenoir cyce (kW)
$\dot{W}_B$	Net Power input to the reversed Brayton cycle (kW)
$\dot{m}$	Mass flow rate of fluid/gas inside the cycle (kg/s)
ϵ_H	Heat Exchanger effectivess of hot side heat exchanger
ϵ_L	Heat Exchanger effectivess of cold side heat exchanger
η_I	Irreversible thermal efficiency for finite time Carnot cycle
η_c	Irreversible compression efficiency
γ	Adiabatic index of the gas
ζ	Reversed Brayton cycle temperature ratio
c_p	Specific heat at constant pressure (kJ/kgK)
c_v	Specific heat at constant volume (kJ/kgK)

Manuscript received January 1, 2025; revised April 5, 2025.

A. Pai is an Associate Professor in the Department of Aeronautical and Automobile Engineering, Manipal Institute of Technology, Manipal Academy of Higher Education, Manipal, Karnataka, India, 576104. (e-mail: anand.pai@manipal.edu).

C. Bekal is an Associate Professor in the Department of Aeronautical and Automobile Engineering, Manipal Institute of Technology, Manipal Academy of Higher Education, Manipal, Karnataka, India, 576104. (e-mail: chandrakantha.bekal@manipal.edu).

M. Shetty is an Assistant Professor in the Department of Aeronautical and Automobile Engineering, Manipal Institute of Technology, Manipal Academy of Higher Education, Manipal, Karnataka, India, 576104. (e-mail: manjunath.shetty@manipal.edu).

B.S. Shenoy is a Professor in the Department of Aeronautical and Automobile Engineering, Manipal Institute of Technology, Manipal Academy of Higher Education, Manipal, Karnataka, India, 576104 (corresponding author to provide phone: +91-8202825482; e-mail: satish.shenoy@manipal.edu).

I. INTRODUCTION

ONE of the latest advancements in thermodynamics is the incorporation of the finite-time concept to account for both internal and external irreversibilities in conventional heat engine and reversed heat engine cycles [1]. Finite Time Thermodynamics (FTT) was found to be applicable to both steady-flow and reciprocating heat engine cycles. It was utilized to compute the real-time efficiency of various processes, including power generation, refrigeration, and heat pump systems [2], [3]. Researchers in this field have explored innovative approaches to maximize energy utilization and minimize losses, making FTT a crucial discipline in the pursuit of sustainable and efficient energy conversion technologies. The Carnot heat engine was modified by several researchers which led to the pioneering work of Curzon and Ahlborn [4] in 1975. The authors provided the irreversible thermal efficiency equation as shown in Eq. 1. Irreversible Carnot cycle is still being investigated by researchers worldwide [5]. Extending the concepts of Curzon-Ahlborn, the Agarwal thermal engine was introduced and subjected to thermodynamic analysis [6].

$$\eta_I = \sqrt{\frac{T_L}{T_H}} \tag{1}$$

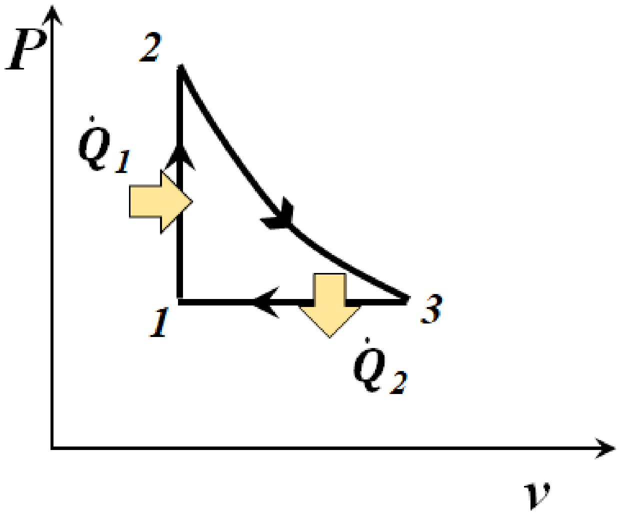

Fig. 1. P-v plot of ideal Lenoir cycle

The Ideal Lenoir cycle is a three-process cycle proposed by Lenoir in 1860 [7], [8], as illustrated in Figure 1. It is a triangular cycle with process 1-2 comprising reversible isochoric heat addition, process 2-3 being reversible adiabatic expansion, and process 3-1, a reversible isobaric heat rejection. Lenoir cycle has practically found applications in pulse-jet engines [9], [10], [11], [12]. Significant research has been done on the finite time Lenoir power cycles for improvement in the thermal efficiency and power optimization by Wang et al. in [13], [14].

Unlike the power generation facilitated by heat engine cycles, applications such as heat pumps and air conditioning demand the use of reversed heat engine cycles [15], [16]. The Vapor Compression Refrigeration cycle (VCR) has been extensively employed in industrial, commercial, and domestic settings for refrigeration and air conditioning. Nevertheless, the dependence on a refrigerant like R134a in VCR cycles results in operating costs for refilling and maintenance. Consequently, there is a growing emphasis on air refrigeration cycles, specifically the reversed Brayton's cycle or Bell-Coleman cycle, which utilizes air as the working fluid [17], [18], [19], [20]. The analysis of finite time reversed Brayton cycles has been conducted in [21], [22], [23]. Ahmadi et al. [24], [25], [26], [27] studied the irreversible refrigeration cycles comprising reversed Sterling, reversed Ericsson, reversed Carnot and multi-heat source irreversible refrigerators with emphasis on cooling effect and coefficient of performance as the parameters. The authors employed the concept of multi-objective optimization for assessing the effect of influencing variables. The variables considered include the ratio of fluid temperatures, heat conductance rates, the effectiveness of the condenser and the evaporator respectively.

The novelty of the current study lies in the parametric analysis of the finite time reversed Lenoir cycle, an aspect not previously investigated for refrigeration and air conditioning applications. The objective of the study was to analyze the coefficient of performance and power input to the cycle as key output parameters. These parameters were influenced by several factors, including the design of the heat exchanger, the properties of the fluid, ambient conditions, and the state values of the reversed Lenoir cycle, which were accounted for in the analysis.

II. Finite Time Reversed Lenoir Cycle

A. *Infinite heat capacity*

The cycle $1-2S-3$ in Figure 2 shows the ideal reversed Lenoir cycle working between two infinite heat capacity, thermal energy reservoirs at T_H and T_L respectively. As shown, $1-2S$ is adiabatic compression, $2S-3$ is isochoric heat rejection, and $3-1$ is isobaric heat addition. The cycle $1-2-3$ shows a finite time reversed Lenoir cycle. Figure 3 shows the components of a reversed Lenoir cycle, which employ regenerative type heat exchangers most suitable for the isochoric processes, while also applicable to isobaric processes [28]. Due to the irreversible losses during the compression caused by entropy generation, friction, heat leakage and other irreversibilities, the state '$2S$' shifts to '2'. These two states can be identified on the P-v and T-s plots in Figure 2. To account for the irreversibilities, an irreverible compression efficiency was introduced as given by Eq. 2.

$$\eta_c = \frac{T_{2S} - T_1}{T_2 - T_1} \tag{2}$$

For the cycle $1-2S-3$, the total entropy change of the gas is zero, in line with the second law of thermodynamics [28]. Since $1-2S$ is an isentropic process, hence $\Delta S_{1\to 2S}$=0.

$$\sum_{i=1}^{3} \Delta S_{i\to i+1} = 0 \tag{3}$$

$$\Delta S_{1\to 2S} + \Delta S_{2S\to 3} + \Delta S_{3\to 1} = 0 \tag{4}$$

$$\Delta S_{2S\to 3} = -\Delta S_{3\to 1} \tag{5}$$

$$\dot{m}c_v ln\left(\frac{T_3}{T_{2S}}\right) = -\dot{m}c_p ln\left(\frac{T_1}{T_3}\right) \tag{6}$$

$$\left(\frac{T_3}{T_{2S}}\right) = \left(\frac{T_3}{T_1}\right)^{\gamma} \tag{7}$$

$$T_3{}^{\gamma-1} = \frac{T_1{}^{\gamma}}{T_{2S}} \tag{8}$$

If 'π' is the pressure ratio $\frac{P_2}{P_1}$ as given in Eq. 9, then Eq. 10 shows the relationship between the temperatures T_1 and T_2, corresponding to the temperatures before and after

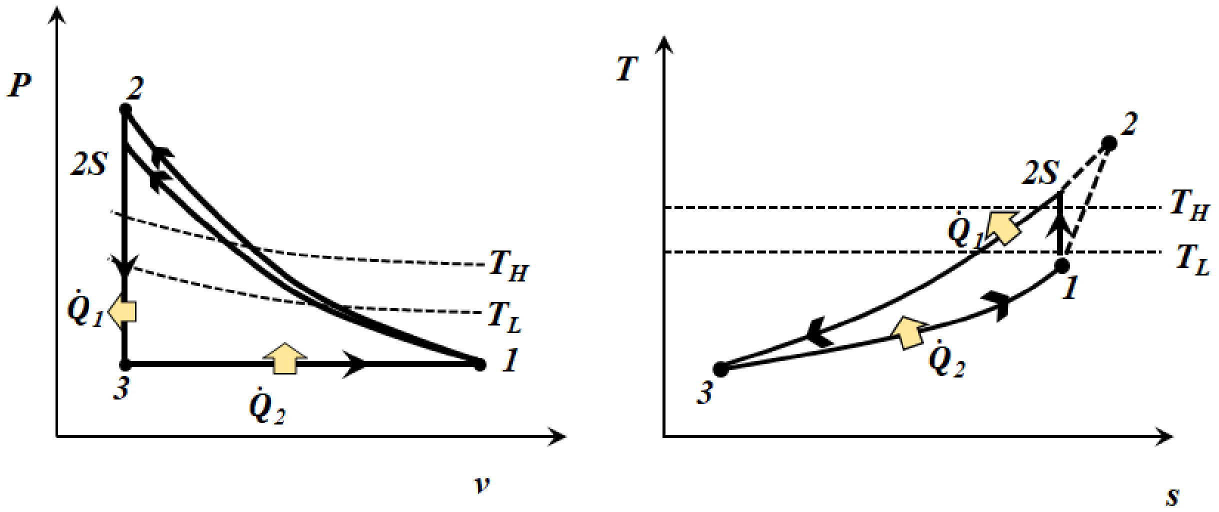

Fig. 2. P-v and T-s plots of an irreversible reversed Lenoir cycle

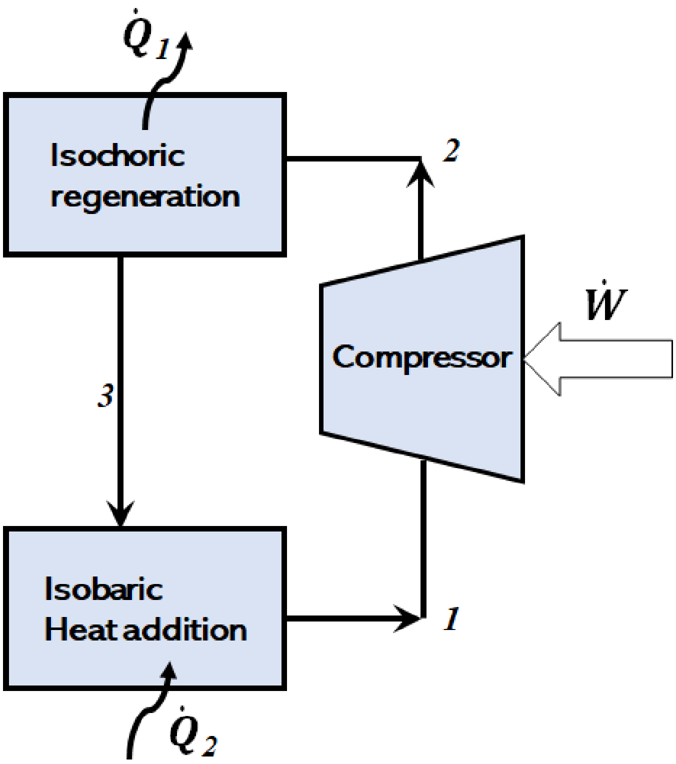

Fig. 3. Components of the Reversed Lenoir cycle

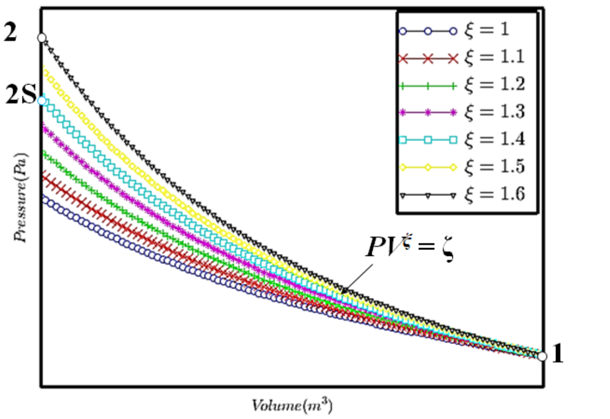

Fig. 4. Compression process for different values of the polytropic index 'ξ'

the irreversible compression. As seen from Figure 4, the reversible adiabatic process $1-2S$, can be considered as a particular case of a polytropic process occurring as per the relation PV$^{\xi}$=ζ, where ξ=γ (γ=1.4 for air and ζ is a constant). When irreversibility occurs during the process, 'ξ' increases as seen in Figure 2 and the radius of curvature decreases for the process curve. Hence, the process 1-2 will occur with the limit $\gamma < \xi$, with higher values of 'ξ' leading to greater irreversibility. From Eq. 2, Eq. 10 and Eq. 11, an expression for η_c is obtained as given in Eq. 12. The range for the pressure ratio has been considered as $4 \leq \pi \leq 7$ [27].

$$\pi = \frac{P_2}{P_1} \tag{9}$$

$$\frac{T_{2S}}{T_1} = \left(\frac{P_{2S}}{P_1}\right)^{\frac{\gamma-1}{\gamma}} = \left(\frac{V_1}{V_{2S}}\right)^{\gamma-1} = \left(\frac{V_1}{V_2}\right)^{\gamma-1} = \pi^{\frac{\gamma-1}{\xi}} \tag{10}$$

$$\frac{T_2}{T_1} = \left(\frac{P_2}{P_1}\right)^{\frac{\xi-1}{\xi}} = \pi^{\frac{\xi-1}{\xi}} \tag{11}$$

$$\eta_c = \frac{\pi^{\frac{\gamma-1}{\xi}} - 1}{\pi^{\frac{\gamma-1}{\gamma}} - 1} \tag{12}$$

From Eq. 8, Eq. 10, and Eq. 11, the Eq. 13 is obtained.

$$T_3 = \left(\pi^{\frac{-1}{\xi}}\right) T_1 = \frac{T_{2S}}{\pi^{\frac{\gamma}{\xi}}} = \frac{T_2}{\pi} \tag{13}$$

For the heat exchangers, the number of transfer units (NTU) is an important design metric given by Eq. 14 and capacity ratio (C_r) given by Eq. 15, respectively.

$$NTU = \frac{UA_s}{C_{min}} \tag{14}$$

$$C_r = \frac{C_{min}}{C_{max}} \tag{15}$$

$$\dot{Q} = UA_s\Delta T_{lm} \tag{16}$$

If a gas is considered the working fluid within the cycle, the heat transfer between the gas and the thermal reservoir by heat convection (Newton's law of cooling) is accounted for. Eq. 17 denotes the heat dissipated during process 2-3 in the hot-side heat exchanger, while Eq. 18 represents the heat added during process 3-1 from the cold-side heat exchanger. The logarithmic mean temperature difference (LMTD) is considered for both heat exchangers in these equations.

$$\dot{Q}_1 = \dot{m}c_v\epsilon_H(T_C - T_H) = U_H A_s \frac{T_2 - T_3}{ln(\frac{T_2 - T_H}{T_H - T_3})} \tag{17}$$

$$\dot{Q}_2 = \dot{m}c_p\epsilon_L(T_L - T_E) = U_L A_s \frac{T_1 - T_3}{ln(\frac{T_1 - T_L}{T_L - T_3})} \tag{18}$$

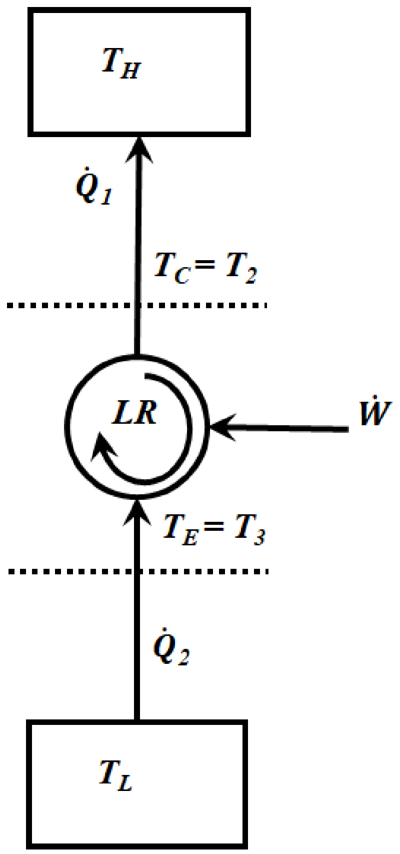

Fig. 5. Schematic of a finite time reversed Lenoir cycle

The number of transfer units for the hot side heat exchanger (N_H) and the cold side heat exchanger (N_L) are given in Eq. 19 and Eq. 20 respectively. The effectiveness of the hot side heat exchanger (ϵ_H) is given by Eq. 21 and that of the cold side heat exchanger (ϵ_L) is given by Eq. 22 respectively, which are popularly used in analysis of heat exchangers [25], [27].

$$N_H = \frac{U_H A_s}{\dot{m}c_v} \tag{19}$$

$$N_L = \frac{U_L A_s}{\dot{m}c_p} = \frac{U_L A_s}{\dot{m}\gamma c_v} \tag{20}$$

$$\epsilon_H = 1 - exp\left(-N_H\right) = 1 - exp\left[\frac{-U_H A_s}{\dot{m}c_v}\right] \tag{21}$$

$$\epsilon_L = 1 - exp\left(-N_L\right) = 1 - exp\left[\frac{-U_L A_s}{\dot{m}\gamma c_v}\right] \tag{22}$$

It is convenient to introduce dimensionless temperature ratios 'a_1','a_2', and 'a_3' for computational purposes. Let $a_1 = \frac{T_3}{T_L} = \frac{T_2}{\pi T_L}$, $a_2 = \frac{T_H}{T_L}$, and $a_3 = \frac{T_2}{T_H}$, then $a_1 = \frac{a_2 a_3}{\pi}$. Using Eq 17, Eq. 18, Eq. 21, and Eq. 22 the following expressions, Eq. 23 and Eq. 24 are obtained relating T_1 and T_2 in terms of T_L and T_H respectively.

$$T_1 = \pi^{\frac{1}{\xi}} T_L \left[1 - \frac{1}{\epsilon_L}\ln\left(\frac{1}{1-\epsilon_L}\right)\frac{a_1(\pi^{\frac{1}{\xi}} - 1)}{\ln\left(\frac{\pi^{\frac{1}{\xi}} - \frac{a_2}{a_1}}{\frac{a_2}{a_1} - 1}\right)}\right] \tag{23}$$

$$T_2 = T_H \left[1 - \frac{a_1}{a_2\epsilon_H}\ln\left(\frac{1}{1-\epsilon_H}\right)\frac{(\pi - 1)}{\ln\left(\frac{\pi - \frac{a_2}{a_1}}{\frac{a_2}{a_1} - 1}\right)}\right] \tag{24}$$

Based on Eq. 17 and Eq. 18, the power input to the reversed Lenoir cycle $\dot{W}$ is given by Eq. 25 and Eq. 26 respectively.

$$\dot{W} = \dot{Q}_1 - \dot{Q}_2 = \dot{m}c_v\left[\epsilon_H(T_2 - T_H) + \gamma\epsilon_L(T_L - T_3)\right] \tag{25}$$

$$\dot{W} = \dot{m}c_v T_L\left[\epsilon_H(\pi a_1 - a_2) + \gamma\epsilon_L(1 - a_1)\right] \tag{26}$$

For any refrigeration cycle, the critical performance parameter is the coefficient of performance ('COP') [27], given by Eq. 27, where COP_{LR} represents the coefficient of performance for the Lenoir Refrigeration cycle.

$$COP_{LR} = \frac{\dot{Q}_2}{\dot{W}} = \frac{\gamma\epsilon_L(1 - a_1)}{\left[\epsilon_H(\pi a_1 - a_2) + \gamma\epsilon_L(1 - a_1)\right]} \tag{27}$$

III. Numerical Studies

A. Fluid properties and ambient conditions

The working fluid within the reversed Lenoir cycle was taken as air, with c_v=0.718 kJ/kgK, γ=1.4 [29]. A nominal flow rate of $\dot{m}$= 1 kg/s was considered for the air flow within the cycle. Generally, an air conditioning application has well-defined temperature limits, 'T_H' can be considered as the ambient atmospheric temperature [30], [31]. Depending on the seasonal variations in tropical areas of the Asia-Pacific, 'T_H' varies between 295 K to 320 K [32]. 'T_L' is the temperature of the refrigerated space, which can be taken as 288 K, the least optimal temperature for human comfort [33]. It is important to note that 'T_2', the peak temperature of the reversed Lenoir cycle is higher than the hot-side reservoir temperature 'T_H' (referring to Figure 2), which infers $a_3 >$

1. The upper limit for a_3 has to be significantly less than 1.1, which would lead to $(T_2 - T_H)$=32 K, which is the difference between the reservoir temperatures. Hence, a nominal value of 1.01 (leading to 3.2 K difference between T_2 and T_H) has been considered as the maximum value of a_3. Accordingly, the following limits of the functions a_2, π, and a_3 are defined :

$$1.02 \leq a_2 \leq 1.11 \tag{28}$$

$$4 \leq \pi \leq 7 \tag{29}$$

$$1.01 \geq a_3 > 1 \tag{30}$$

Since summer is the most demanding season for air-conditioning, the maximum value of a_2=1.11 was considered. a_1 is a function of the a_2, a_3 and pressure ratio 'π'. Hence, π= 4, 5, 6, and 7 were taken up for the parametric studies.

B. Heat Exchanger Parameters

The heat exchangers, namely the cold side heat exchanger and the hot side heat exchanger, in air conditioning applications can be classified as low-temperature range heat exchangers [34]. As per Pacio et al. [34], for single working fluid heat exchangers, regenerative type is considered the most optimal one, with heating surface density up to 6500 m^2. In the current study, assuming that both the heat exchangers have equal cross-sectional area 'A_s', a nominal value of 100 m^2 was considered for the small-scale heat exchanger. Since air was used as the working fluid in the reversed Lenoir cycle, it was also the fluid on the opposite side of both heat exchangers for removal of heat. Hence, the overall heat transfer coefficients U_H and U_L have to be considered for air-air convective heat transfer, which range from 10-30 W/m^2K [35], [36], [37]. As per the classical thermodynamics and heat transfer principles, the convective heat transfer coefficient depends on the viscosity, the thermal conductivity, and the specific heat of the fluids transferring the heat. The specific heat of air decreases with increase in temperature, lowering the overall heat transfer coefficient. Hence, $U_L > U_H$. Table I shows the variation of the heat exchanger effectiveness ϵ_H and ϵ_L with the overall heat transfer coefficients U_L and U_H.

TABLE I
VARIATION OF THE HEAT EXCHANGER EFFECTIVENESS WITH OVERALL HEAT TRANSFER COEFFICIENTS

U_L (W/m^2K)	U_H (W/m^2K)	A_s (m^2)	ϵ_L	ϵ_H
30	27	100	0.949	0.932
27	24	100	0.932	0.908
24	21	100	0.908	0.876
21	18	100	0.876	0.833
18	15	100	0.833	0.775
15	12	100	0.775	0.697
12	9	100	0.697	0.592

Each set of computed values for ϵ_H and ϵ_L are taken up against each value of the pressure ratio π, the power $\dot{W}$ and COP_{LR} are determined, and the effect of the parameters on the output is analyzed.

C. Comparison with Finite Time Reversed Brayton Cycle

Reversed Brayton cycles are popular air refrigeration cycles in which the refrigerant (air) enters the compressor at 1', undergoes compression to 2', rejects the heat '$\dot{Q}_{H_B}$' at constant pressure to a sink of infinite heat capacity till 3', expands in the turbine upto state 3', and finally is heated isobarically, adding heat '$\dot{Q}_{L_B}$', till 1' to complete one cycle. The finite time reversed Brayton cycle 1'-2'-3'-4'-1' is shown in the P-v and T-s plots of Figure 6. The states 1-2-3-1 on the P-v plot represent the finite time reversed Lenoir cycle. It is evident from the P-v plot that for the same mass flow rate of the working fluid, the cycle times for reversed Brayton cycle is much higher than that of the reversed Lenoir cycle owing to the additional area under the P-v diagram 2'-3'-4'. Hence, if the cycle times have to be kept the same, then the air mass flow rate is case of the reversed Brayton cycle has to be twice that of the reversed Lenoir cycle. In the current comparison, the internal irreversibility effects due to certain losses like irreversible compression and expansion, pressure drop, frictional effects etc. in the Brayton cycle are ignored. The equations used in the parametric characterization of reversed Brayton cycle conducted by Tyagi and others [38], [39] are shown in Eq's 31,32, 33, 34, 35 and 36. To compare the finite time reversed Lenoir cycle with the finite time reversed Brayton cycle, the hot-side heat exchanger effectiveness ϵ_H = 0.592 - 0.932 and cold-side heat exchanger effectiveness ϵ_L = 0.697 - 0.949, and the pressure ratios π = 4, 5, 6, and 7 were considered. The thermal reservoir temperatures were taken as T_H = 320 K and T_L = 288 K, respectively.

$$T_{3'} = \frac{\zeta(1-\epsilon_H)\epsilon_L T_L + \epsilon_H T_H}{\zeta[1-(1-\epsilon_H)(1-\epsilon_L)]} \tag{31}$$

$$T_{3'} = (-\epsilon_L)\epsilon_H T_H + \zeta \epsilon_L T_L \tag{32}$$

Where

$$\zeta = \frac{T_{3'}}{T_{2'}} = \frac{T_{4'}}{T_{1'}} = \pi^{\frac{\gamma-1}{\gamma}} \tag{33}$$

$$\dot{Q}_{L_B} = \frac{C_{air}\epsilon_H \epsilon_L(\zeta T_L - T_H)}{\zeta[1-(1-\epsilon_H)(1-\epsilon_L)]} \tag{34}$$

$$\dot{W}_B = \dot{Q}_{H_B} - \dot{Q}_{L_B} = \frac{C_{air}\epsilon_H \epsilon_L(\zeta T_L - T_H)(\zeta - 1)}{\zeta[1-(1-\epsilon_H)(1-\epsilon_L)]} \tag{35}$$

$$COP_B = \frac{\dot{Q}_L}{\dot{W}_B} = \frac{1}{\zeta - 1} \tag{36}$$

IV. Analysis and Discussion

The variation of the input power for the finite time, reversed Lenoir cycle is shown in Figure 7 with the different parameters, respectively. At a given pressure ratio 'π', the power $\dot{W}$ increased as the heat exchanger effectiveness values of ϵ_L and ϵ_H increased, with a constant gap across the curves with different pressure ratios for a given set of the effectiveness values. Also, the increase in pressure ratio π led to an increase in the power requirement $\dot{W}$.

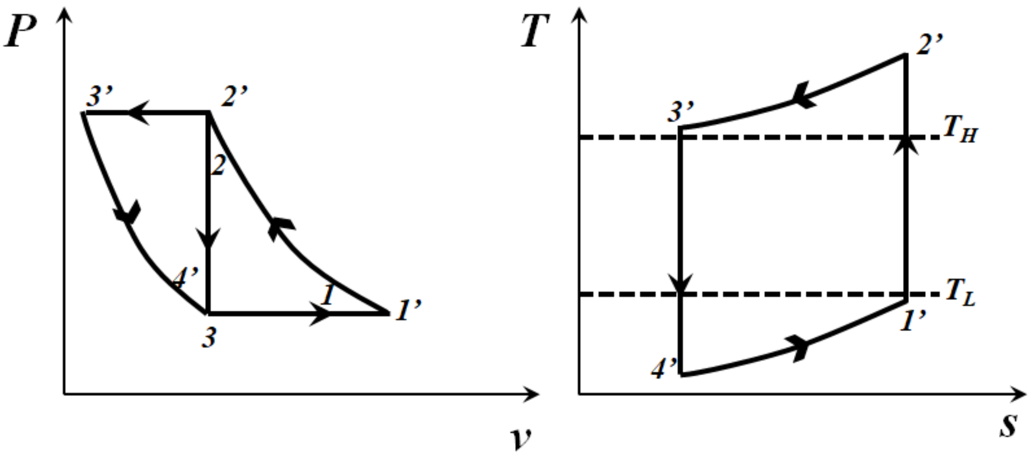

Fig. 6. Schematic of a finite time reversed Brayton cycle

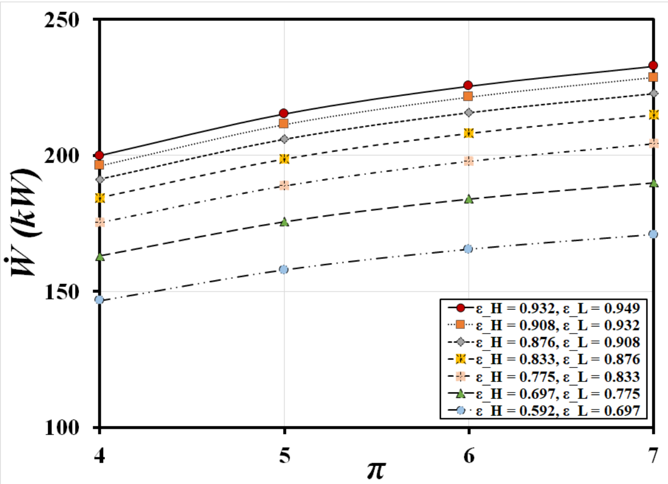

Fig. 7. Variation of the required power $\dot{W}$ with pressure ratio π for the reversed Lenoir cycle

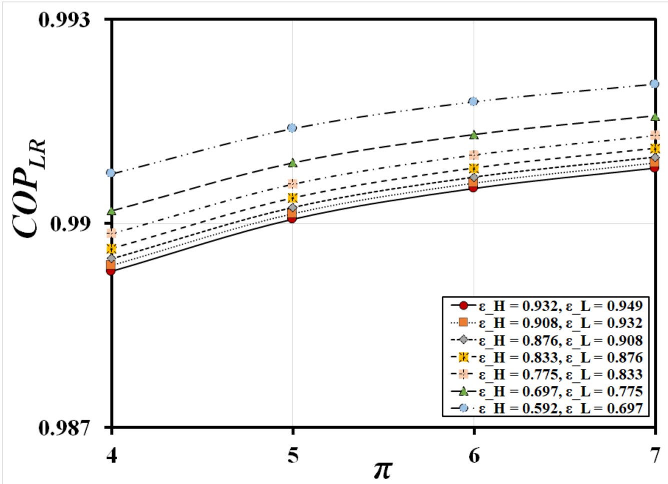

Fig. 8. Variation of COP_{LR} for the reversed Lenoir cycle with pressure ratio π

Figure 8 shows the variation of COP_{LR} with the pressure ratio π and the different values of the heat exchanger effectiveness ϵ_L and ϵ_H respectively. With increase in the heat exchanger effectiveness (ϵ_H and ϵ_L), there was a decrease in the COP_{LR}, with highest value of 0.992 for π=4, ϵ_H=0.592, and ϵ_L=0.697. At given set of the heat exchanger effectiveness values, as the pressure ratio π increased from 4 to 7, the COP_{LR} also increased, the magnitude of improvement was significant in case of lower values of ϵ_H and ϵ_L.

From Figure 9, as there is a switch over to lower values of the heat exchanger effectiveness, the power requirement $\dot{W}$ decreased, while (COP_{LR}) was found to increase slightly. Notably, at lowest values of ϵ_H and ϵ_L, COP_{LR} remained almost the same, but the power requirement $\dot{W}$ increases, highlighting that with continuous operation, the reversed Lenoir cycle would give lesser cooling effect for the same power. In Figure 10, for $\epsilon_H = 0.932$ and $\epsilon_L = 0.949$, the COP_{LR} is found to increase linearly with $\dot{W}$, as the pressure ratio π increases from 4 to 7.

As the values of the heat exchanger effectiveness ϵ_H and ϵ_L decrease, both the coefficient of performance (COP_{LR}) of the finite time reversed Lenoir cycle and the power requirement $\dot{W}$ were found to decrease. This trend is clearly illustrated in Figure 11, Figure 12, Figure 13, Figure 14, Figure 15, and Figure 16, respectively. Over continuous operation, heat exchangers are prone to deterioration due to factors such

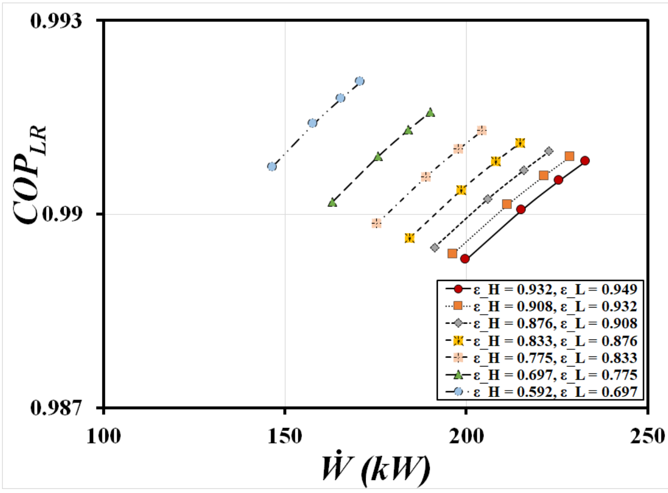

Fig. 9. Variation of COP_{LR} for the reversed Lenoir cycle with the power

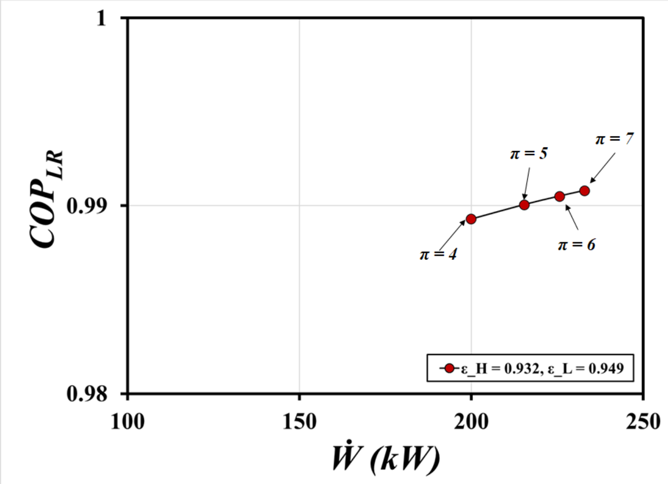

Fig. 10. Variation of the COP for the reversed Lenoir cycle with the power at $\epsilon_H = 0.932, \epsilon_L = 0.949$

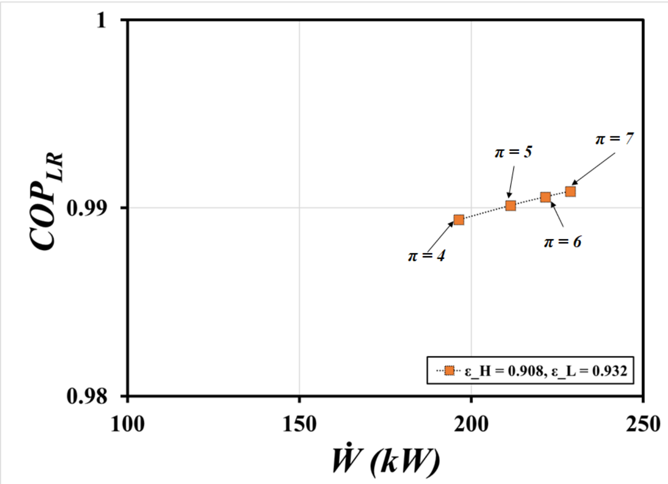

Fig. 11. Variation of the COP for the reversed Lenoir cycle with the power at $\epsilon_H = 0.908, \epsilon_L = 0.932$

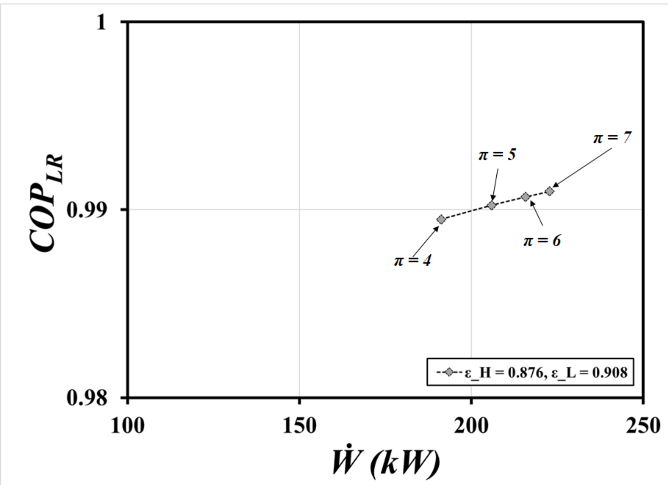

Fig. 12. Variation of the COP for the reversed Lenoir cycle with the power at $\epsilon_H = 0.876, \epsilon_L = 0.908$

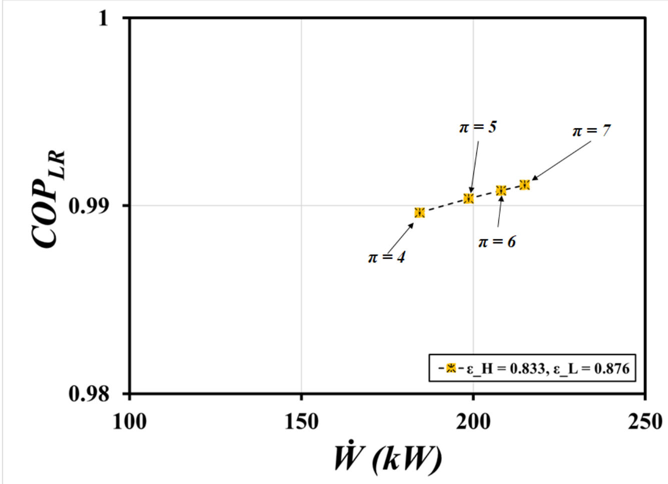

Fig. 13. Variation of the COP for the reversed Lenoir cycle with the power at $\epsilon_H = 0.833, \epsilon_L = 0.876$

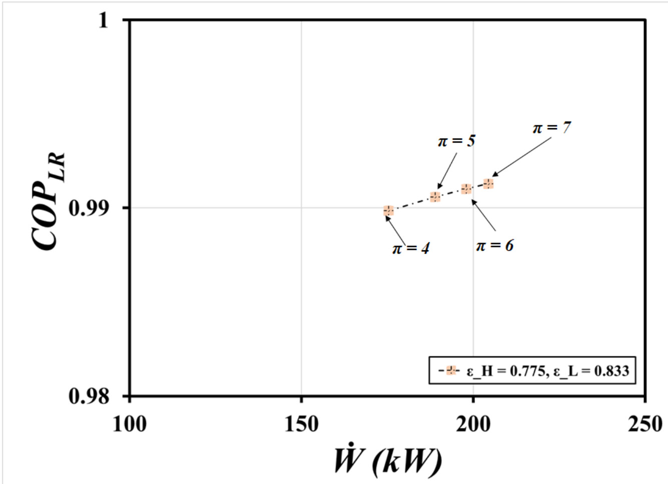

Fig. 14. Variation of the COP for the reversed Lenoir cycle with the power at $\epsilon_H = 0.775, \epsilon_L = 0.833$

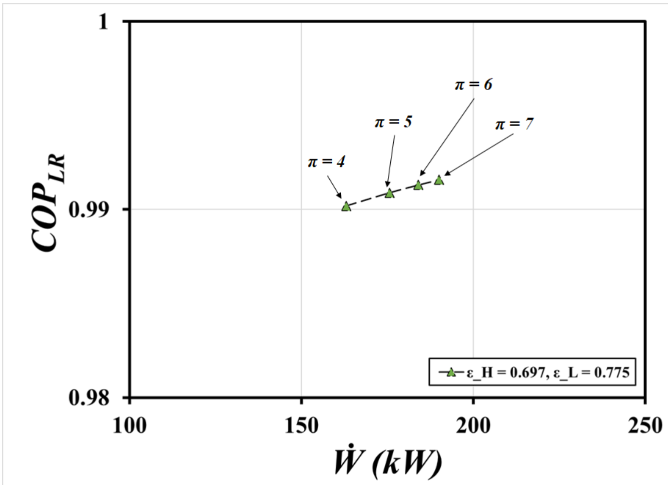

Fig. 15. Variation of the COP for the reversed Lenoir cycle with the power at $\epsilon_H = 0.697, \epsilon_L = 0.775$

as scaling, deposition, and blockage of cooling lines, which further degrade performance. These findings highlight the critical need for regular maintenance and cleaning protocols to combat fouling and ensure sustained efficiency of the reversed Lenoir cycle in practical applications.

Table II shows the values of η_c for different values of π and ξ. Thus, it is seen that η_c is a major function of ξ than π, highest value of 'η_c'= 0.761 is seen as ξ=1.5 and π=4

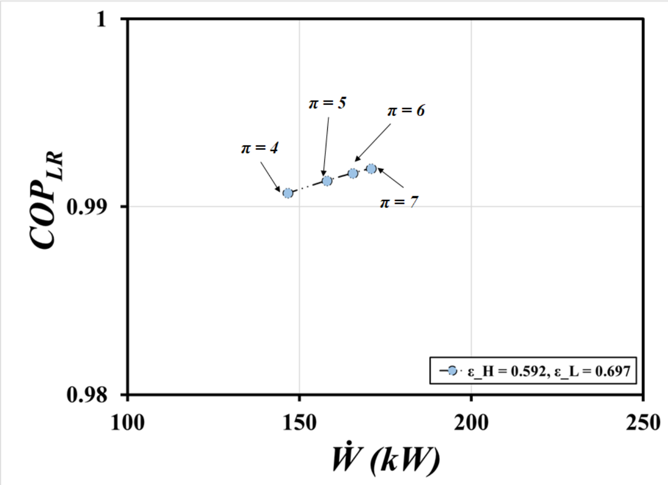

Fig. 16. Variation of the COP for the reversed Lenoir cycle with the power at $\epsilon_H = 0.592, \epsilon_L = 0.697$

TABLE II
VARIATION OF THE IRREVERSIBLE COMPRESSION EFFICIENCY η_c WITH π AND ξ VALUES

π	ξ	γ	η_c
4	1.50	1.4	0.761
4	1.60	1.4	0.608
4	1.70	1.4	0.501
4	1.80	1.4	0.424
5	1.50	1.4	0.755
5	1.60	1.4	0.598
5	1.70	1.4	0.490
5	1.80	1.4	0.412
6	1.50	1.4	0.750
6	1.60	1.4	0.590
6	1.70	1.4	0.481
6	1.80	1.4	0.402
7	1.50	1.4	0.745
7	1.60	1.4	0.583
7	1.70	1.4	0.473
7	1.80	1.4	0.394

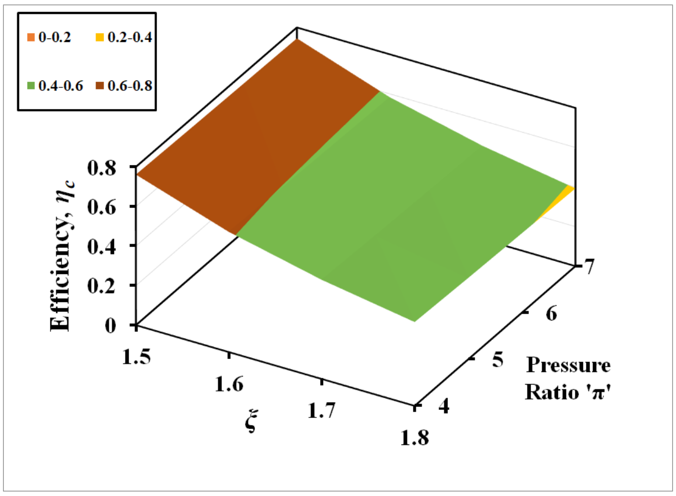

Fig. 17. Surface Plot of the irreversible efficiency η_c

(2 being closest to $2S$). This indicates that the effect of the internal and external irreversibilities is to increase the value of ξ which consequently reduces the value of η_c up to 0.394 (for ξ=1.8 and π=7). Figure 17 shows the 3D surface plot of the irreversible efficiency η_c, which indicates that at lower values of ξ, the efficiency increases.

A. *Comparison with finite time reversed Brayton cycle*

The comparative analysis between the two reversed finite-time cycles, Brayton and Lenoir, was conducted. The power inputs to the cycles are depicted in Figure 18 (a) and Figure 18 (b), respectively. The reversed Brayton cycle clearly showed lower requirements of input power $\dot{W}_B$ compared to the reversed Lenoir cycle. Increasing the heat exchanger effectiveness on both the hot-side and cold-side heat exchangers resulted in an elevated power input to the reversed Brayton cycle across all pressure ratio (π) values, while that for the Reversed Lenoir cycle exhibited a corresponding decrease in the power input. For heat exchanger effectiveness $\epsilon_H = 0.592$ and $\epsilon_L = 0.697$, at $\pi = 4.0$, the power input to the reversed Brayton cycle was 33.42 kW, compared to 146.59 kW for the reversed Lenoir cycle. As the pressure ratio π increased from 4.0 to 7.0, the power input to the reversed Brayton cycle as well as that of the reversed Lenoir cycle showed an increase. Therefore, the Reversed Lenoir cycle can maintain stable performance during continuous operation, as a reduction in heat exchanger effectiveness lowers the power input.

The coefficients of performance (COPs) for the cycles are illustrated in Figure 19 (a) and Figure 19 (b), respectively at the respective effectiveness values of the hot-side and cold-side heat exchangers. The COP of the reversed Brayton cycle 'COP_B' was found to be a strong function of the pressure ratio 'π', while being largely independent on the heat exchanger effectiveness values (ϵ_H and ϵ_L). Conversely, the COP of the reversed Lenoir cycle COP_{LR} was largely independent of the pressure ratio 'π' as well as the heat exchanger effectiveness values. At $\pi = 4.0$ and $\epsilon_H = 0.592$, $\epsilon_L = 0.697$, COP_B was 2.05, whereas COP_{LR} was $\sim$ 0.991. Lower heat exchanger effectiveness was further examined for comparison between the two cycles. For $\epsilon_H = 0.592$, $\epsilon_L = 0.697$, it was deduced that the reversed Brayton cycle, with a lower power input at $\pi = 4.0$ and $COP_B = 2.05$, would yield a desired cooling effect of 68.5 kW, whereas the reversed Lenoir cycle would provide a cooling effect of 145.23 kW, more than twice as that of the former, but with almost double the input power requirement. However, at $\pi = 7.0$, the power input of the reversed Brayton cycle increased to 73.53 kW, with COP_B dropping to 1.34, resulting in a cooling effect of 98.53 kW ($\sim$ 43.8% increase compared to 'π=4). In contrast, the cooling effect of the reversed Lenoir cycle increased slightly to 169.46 kW ($\sim$ 16.78% increase compared to 'π=4). Hence, there exists a trade-off between the two cycles in terms of cooling effect and power input. However, it is worth noting that the reversed Lenoir cycle maintains a stable COP as 'π' increases, even as the heat exchangers experience periodic deterioration (such as scaling and deposits on the fins and tubes) thereby sustaining its performance. In contrast, while the performance of the reversed Brayton cycle is largely unaffected by heat exchanger effectiveness, its COP decreases with increasing values of 'π'.

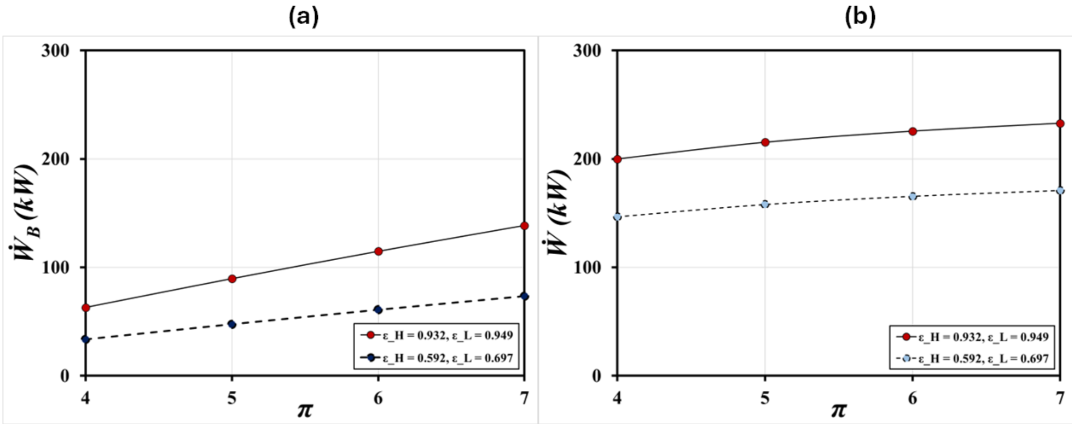

Fig. 18. Power input comparison for the (a) Finite time reversed Brayton cycle (b) Finite time reversed Lenoir cycle

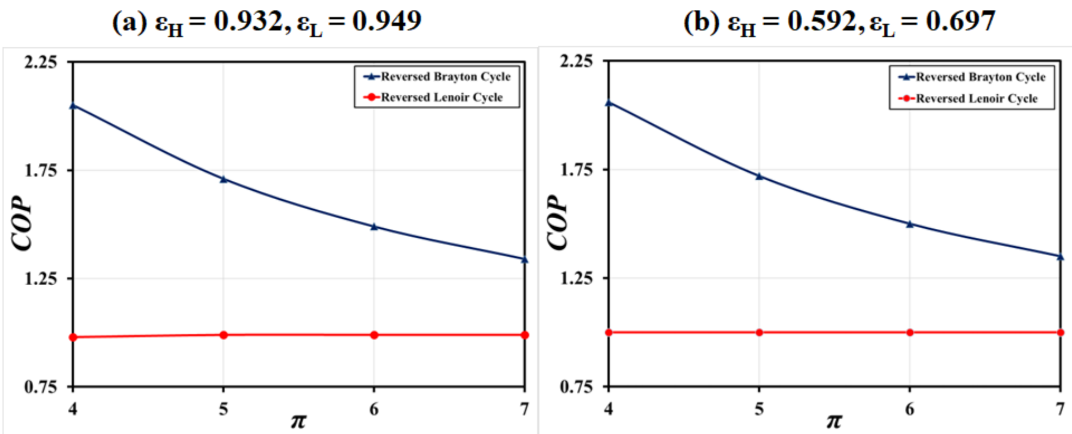

Fig. 19. Comparison of the COP's for finite time reversed Brayton cycle and reversed Lenoir cycle at (a) ϵ_H= 0.932, ϵ_L= 0.949 (b)ϵ_H= 0.592, ϵ_L= 0.697

V. Conclusions

In the present study, a parametric analysis of the finite-time reversed Lenoir cycle for refrigeration and air conditioning applications was conducted. To account for losses during compression, the irreversible compression efficiency was considered, delineating the states '2' and '$2S$'. Infinite heat capacity thermal energy reservoirs at temperatures T_H (hot-side) and T_L (cold-side) were considered during the study. During performance optimization, the impact of heat exchanger effectiveness, and other factors on the coefficient of performance and power input to the reversed Lenoir cycle were analyzed. A maximum COP_{LR} of 0.992 was noticed at ϵ_H=0.592 and ϵ_L=0.697. The reduction in heat exchanger effectiveness decreased the power requirement, while maintaining a stable value of the coefficient of performance. As pressure ratio π increased, COP_{LR} was found to increase slightly, while the power requirement $\dot{W}$ was found to increase significantly. The compression efficiency η_c was a strong function of the index ξ than the pressure ratio π, and its maximum value was > 0.761, when $\xi \sim 1.5$, i.e. the internal and external irreversibilities at their lowest (2 closest to $2S$).

The reversed Lenoir cycle demonstrated a superior cooling effect compared to the reversed Brayton cycle, even with lower heat exchanger effectiveness. However, as the pressure ratio increased, the cooling performance of the reversed Brayton cycle improved significantly relative to the Lenoir cycle. While the Lenoir cycle provided higher cooling output, it required twice the power input, though it maintained a stable coefficient of performance largely independent of both the pressure ratio and heat exchanger effectiveness (on both the hot and cold sides). Additionally, during continuous operation, the reversed Lenoir cycle offered consistent performance. It is a three-process cycle, compared to the four-process reversed Brayton cycle. This presents a size advantage, making a reversed Lenoir cycle more compact.

References

[1] S. C. Kaushik, S. K. Tyagi, and P. Kumar, "Finite time thermodynamics of power and refrigeration cycles," Springer, first edition, New Delhi, 2017.

[2] R. DiPippo, "Ideal thermal efficiency for geothermal binary plants," *Geothermics*, vol. 36, no. 3, pp. 276–285, 2007.

[3] D. C. Agrawal, "A simplified version of the Curzon-Ahlborn engine," *European Journal of Physics*, vol. 30, no. 5, pp. 1173–1179, 2009.

[4] F. L. Curzon and B. Ahlborn, "Efficiency of a Carnot engine at maximum power output," *American Journal of Physics*, vol. 43, no. 1, pp. 22–24, 1975.

[5] L. Chen, Z. Meng, Y. Ge, and F. Wu, "Performance analysis and optimization for irreversible combined Carnot heat engine working with ideal quantum gases," *Entropy*, vol. 23, no. 5, p. 536, 2021.

[6] R. T. Paéz-Hernández, J. C. Chimal-Eguía, N. Sánchez-Salas, and D. Ladino-Luna, "General properties for an Agrawal thermal engine," *Journal of Non-Equilibrium Thermodynamics*, vol. 43, no. 2, pp. 131–139, 2018.

[7] L. C. Lichty, "Combustion engine processes," McGraw-Hill, Sixth edition, New York, 1967.

[8] D. P. Georgiou, "Useful work and the thermal efficiency in the ideal Lenolr cycle with regenerative preheating," *Journal of Applied Physics*, vol. 88, no. 10, pp. 5981–5986, 2000.

[9] V. I. Bogdanov. "Interaction of masses in the operating process of pulse jet engines as a means of increasing their thrust efficiency," *Journal of Engineering Physics and Thermophysics*, vol. 79, no. 3, pp. 506-511, 2006.

[10] K Sainath, Ruhail Masood, Mohd Salahuddin, Md Ismail, Mohd Khaleel Ullah, and Mohd Ashraf Ali. An investigation report and design of pulse jet engine. *Int. J. Mechan. Eng. Inform. Technol*, vol. 2, no. 11, pp. 859-866, 2014.

[11] M. Trancossi, O. Mohammedalamin, J. Pascoa, and F. Rodrigues, "Thermodynamic analysis and preliminary design of the cooling system of a pulsejet for aeronautic propulsion," *International Journal of Heat and Technology*, vol. 34, no. 2, pp. S528–S534, 2016.

[12] M. Liu, L. Yu, and W. X. Cai, "Experiment analysis of combustion performance in pulse jet engine," *Energy Procedia*, vol. 100, pp. 248–252, 2016.

[13] R. Wang, L. Chen, Y. Ge, and H. Feng, "Optimizing power and thermal efficiency of an irreversible variable-temperature heat reservoir Lenoir cycle," *Appl. Sci.*, vol. 11, no. 15, 2021.

[14] R. Wang, Y. Ge, L. Chen, H. Feng, and Z. Wu, "Power and thermal efficiency optimization of an irreversible steady-flow Lenoir cycle," *Entropy*, vol. 23, no. 4, pp. 1–11, 2021.

[15] X. Wu, L. Chen, Y. Ge, and F. Sun, "Local stability of an endoreversible heat pump with linear phenomenological heat transfer law working in an ecological regime," *Scientia Iranica*, vol. 19, no. 6, pp. 1519–1525, 2012.

[16] S. Huang, S. Ding, S. Yuan, M. Li, Y. Tan, F. Yue, and S. Dang, "A detection method combining machine vision and resistance analysis for the wiring harnesses of refrigerator temperature sensors," *IAENG International Journal of Computer Science*, vol. 51, no. 6, pp. 703-708, 2024.

[17] H.-M. Chang, M. J. Chung, M. J. Kim, and S. B. Park, "Thermodynamic design of methane liquefaction system based on reversed-Brayton cycle," *Cryogenics*, vol. 49, no. 6, pp. 226–234, 2009.

[18] A. Biglia, L. Comba, E. Fabrizio, P. Gay, A. Mannini, A. Mussinatto, and D. R. Aimonino, "Reversed Brayton cycle for food freezing at very low temperatures: Energy performance and optimisation," *International Journal of Refrigeration*, vol. 81, pp. 82–95, 2017.

[19] L. Wang, H. Li, and J. Zhou, "Thermodynamic investigation of a centrifugal reverse Brayton cycle for refrigeration in air conditioning field," *International Journal of Refrigeration*, vol. 152, pp. 176-191, 2023.

[20] L. Shuailing, M. Guoyuan, X. Shuxue, G. Yuexuan, J. Xiaoya, and W. Guoqiang, "A review of reverse Brayton air cycle refrigerators," *International Journal of Refrigeration*, vol. 150, pp. 200–214, 2023.

[21] L. Chen, N. Ni, G. Cheng, F. Sun, and C. Wu, "Performance analysis for a real closed regenerated Brayton cycle via methods of finite-time thermodynamics," *International Journal of Ambient Energy*, vol. 20, no. 2, pp. 95–104, 1999.

[22] Z. Zhang, L. Chen, and F. Sun, "Energy performance optimization of combined Brayton and two parallel inverse Brayton cycles with regeneration before the inverse cycles," *Scientia Iranica*, vol. 19, no. 5, pp. 1279–1287, 2012.

[23] S. C. Kaushik, S. K. Tyagi, and P. Kumar, "Finite time thermodynamics of Brayton refrigeration cycle," *Finite Time Thermodynamics of Power and Refrigeration Cycles*, pp. 219–240, 2017.

[24] M. H. Ahmadi, M. A. Ahmadi, A. H. Mohammadi, M. Feidt, and S. M. Pourkiaei, "Multi-objective optimization of an irreversible Stirling cryogenic refrigerator cycle," *Energy Conversion and Management*, vol. 82, pp. 351–360, 2014.

[25] M. H. Ahmadi, M. A. Ahmadi, and S. A. Sadatsakkak, "Thermodynamic analysis and performance optimization of irreversible Carnot refrigerator by using multi-objective evolutionary algorithms (MOEAs)," *Renewable and Sustainable Energy Reviews*, vol. 51, pp. 1055–1070, 2015.

[26] M. H. Ahmadi and M. A. Ahmadi, "Multi-objective optimization of performance of three-heat-source irreversible refrigerators based algorithm NSGAII," *Renewable and Sustainable Energy Reviews*, vol. 60, pp. 784–794, 2016.

[27] M. H. Ahmadi, M.-A. Ahmadi, F. Pourfayaz, and M. Bidi, "Thermodynamic analysis and optimization for an irreversible heat pump working on reversed Brayton cycle," *Energy Conversion and Management*, vol. 110, pp. 260–267, 2016.

[28] J. Fricker and A. Zoughaib, "Simultaneous heating and cooling production devices composed by reverse cycle systems under variable loads," *International Journal of Refrigeration*, vol. 55, pp. 1–16, 2015.

[29] E. W. Lemmon, R. T. Jacobsen, S. G. Penoncello, and D. G. Friend, "Thermodynamic properties of air and mixtures of nitrogen, argon, and oxygen from 60 to 2000 K at pressures to 2000 MPa," *Journal of Physical and Chemical Reference Data*, vol. 29, no. 3, pp. 331–385, 2000.

[30] M. Mohanraj, S. Jayaraj, and C. Muraleedharan, "Applications of artificial neural networks for refrigeration, air-conditioning and heat pump systems—a review," *Renewable and Sustainable Energy Reviews*, vol. 16, no. 2, pp. 1340–1358, 2012.

[31] L. Yang, S. Deng, G. Fang, and W. Li, "Improved indoor air temperature and humidity control using a novel direct-expansion-based air conditioning system," *Journal of Building Engineering*, vol. 43, p. 102920, 2021.

[32] A. Asif, M. Zeeshan, and M. Jahanzaib, "Indoor temperature, relative humidity and CO2 levels assessment in academic buildings with different heating, ventilation and air-conditioning systems," *Building and Environment*, vol. 133, pp. 83–90, 2018.

[33] W. Cui, G. Cao, J. H. Park, Q. Ouyang, and Y. Zhu, "Influence of indoor air temperature on human thermal comfort, motivation and performance," *Building and Environment*, vol. 68, pp. 114–122, 2013.

[34] J. C. Pacio and C. A. Dorao, "A review on heat exchanger thermal hydraulic models for cryogenic applications," *Cryogenics*, vol. 51, no. 7, pp. 366–379, 2011.

[35] E. Sparrow, J. Gorman, and J. Abraham, "Quantitative assessment of the overall heat transfer coefficient U," *ASME Journal of Heat Transfer*, vol. 135, no. 6, pp. 1-7, 2013.

[36] M. Amiraslanpour, J. Ghazanfarian, H. Nabaei, and M. H. Taleghani, "Evaluation of laminar airflow heating, ventilation, and air conditioning system for particle dispersion control in operating room including staffs: A non-Boussinesq Lagrangian study," *Journal of Building Physics*, vol. 45, no. 2, pp. 236–264, 2021.

[37] S. A. Zavattoni, L. Cornolti, R. Puragliesi, E. Arrivabeni, A. Ortona, and M. C. Barbato, "Conceptual design of an innovative gas-gas ceramic compact heat exchanger suitable for high temperature applications," *Heat and Mass Transfer*, vol. 60, pp. 1979–1990, 2022.

[38] S. K. Tyagi, G. M. Chen, Q. Wang, and S. C. Kaushik, "A new thermoeconomic approach and parametric study of an irreversible regenerative Brayton refrigeration cycle," *International Journal of Refrigeration*, vol. 29, no. 7, pp. 1167–1174, 2006.

[39] S. C. Kaushik, P. Kumar, and S. Jain, "Finite time thermodynamic optimisation of an irreversible heat pump system using the Lagrangian multiplier method," *International Journal of Ambient Energy*, vol. 22, no. 2, pp. 105-112, 2011.